Article

Not peer-reviewed version

Barium Titanate Synthesis in Water Vapor: From Mechanism to Ceramics Properties

Anastasia Kholodkova *, Yurii Ivakin, Marina Danchevskaya, Galina Muravieva, Alexander Egorov, Aleksey Smirnov, Arseniy Khrustalev, Levko Arbanas, Viktoria Bazarova, Andrey Smirnov

Posted Date: 26 January 2024

doi: 10.20944/preprints202401.1870.v1

Keywords: barium titanate; synthesis in water vapor; topochemical reaction; solid-state reaction; low-frequency dielectric ceramics; conventional ceramics technique; ceramics microstructure; dielectric constant; dielectric loss tangent

Article

Barium Titanate Synthesis in Water Vapor: From Mechanism to Ceramics Properties

Anastasia A. Kholodkova [1,2,*], Yurii D. Ivakin [2,3], Marina N. Danchevskaya [2], Galina P. Muravieva [2], Alexander V. Egorov [2], Aleksey D. Smirnov [4], Arseniy N. Khrustalev [1], Levko A. Arbanas [1], Viktoria E. Bazarova [1] and Andrey V. Smirnov [1]

[1] Laboratory of Ceramic Materials and Technology, MIREA – Russian Technological University, 119454 Moscow, Russia; lywn@yandex.ru (A.N.K), levko147@icloud.com (L.A.A.), bazarovave@yandex.ru (V.E.B.), smirnoff-andrey2009@yandex.ru (A.V.S.)

[2] Chemistry Department, Lomonosov Moscow State University, 119991 Moscow, Russia; mardan@kge.msu.ru (M.N.D.), galina.p.muravyeva@gmail.com (G.P.M.), egorov@kge.msu.ru (A.V.E.)

[3] Mobile Solutions Engineering Center, MIREA – Russian Technological University, 119454 Moscow, Russia, ivakin@kge.msu.ru (Y.D.I.)

[4] Moscow Polytech, 107023 Moscow, Russia; alex-smv99@yandex.ru (A.D.S)

* Correspondence: anastasia.kholodkova@gmail.com

Abstract: A facile and environmentally benign method for a single-phase barium titanate synthesis in water vapor medium was studied to reveal the mechanism of phase transformation of the initial simple oxides mixture and estimate the capability of the product to be used as a raw material for low-frequency dielectric ceramics. The composition and structure of the reaction mixture treated in vapor at 130…150 °C as well as 230 °C for various time were investigated by means of XRD, SEM, HRTEM, EDX, and FTIR methods. The kinetics of the occurring phase transformation was described by Johnson-Mehl-Avrami-Erofeev equation. The reaction between the initial oxides was considered as a topochemical process with an apparent activation energy of 74…80 kJ mol^{-1}. A crucial role in this process belonged to the water vapor medium, which facilitated the generation of the reaction zone and its spreading inward the solid particles. The synthesized tetragonal barium titanate powder (mean particle size of 135 ± 24 nm) was sintered by a conventional technique at 1250 °C to obtain ceramics with grains of about 2 μm. Capacitance measurements performed a dielectric constant and loss tangent of ceramics, which reached 3879 and 6.7 10^{-3}, respectively, at 1 kHz and room temperature.

Keywords: barium titanate; synthesis in water vapor; topochemical reaction; solid-state reaction; low-frequency dielectric ceramics; conventional ceramics technique; ceramics microstructure; dielectric constant; dielectric loss tangent

1. Introduction

Barium titanate is a highly demanded material for a wide area of applications including production of ferro- and piezoelectric ceramics [1,2] and composites [3,4] as well as optoelectronic devices [5], thermistors [6], semiconductors [7], transducers [8], photocatalysts [9,10], coatings [11], and products for biomedicine [12,13]. A key feature of such a versatile application of $BaTiO_3$ is ability of its crystals to perform spontaneous polarization in a temperature range below 120 °C, which is known as its Curie point. $BaTiO_3$ possesses a typical perovskite structure with a sequence of phase transitions: cubic to tetragonal (120…130 °C), tetragonal to orthorhombic (about 5 °C), orthorhombic to rhombohedral (about -90 °C) [14]. Besides the cubic modification, the mentioned phases demonstrate ferroelectric properties due to their spontaneous polarization, among which the most prominent are reported for the tetragonal $BaTiO_3$. A vivid example of this was reported in [15] for $BaTiO_3$ ceramics produced by spark plasma sintering with a room-temperature dielectric constant up to 60000 and low losses of about 0.07.

 doi:10.20944/preprints202401.1870.v1

The methods of $BaTiO_3$ powder production are mostly focused on the needs of multilayer ceramic capacitor (MLCC) industry as it remains the largest consumer of barium titanate. A wide variety of approaches in solid-state as well as wet chemistry have been developed to produce highly pure single-phase $BaTiO_3$ powders with a narrow size distribution and smooth particle shape [16–18]. The groups of solid-state [19,20], mechanochemical [21–23], complexation [24–28], co-precipitation [29,30], sol-gel [31], and hydrothermal [32–34] techniques for obtaining $BaTiO_3$ took their rightful place in laboratories as well as in industry of various scales. Besides the properties of the final product, there are different factors to concern when choosing strategies for $BaTiO_3$ powders production, such as energy consumption, the availability and cost of the initial substances, the complexity of the equipment and its service, and the environmental impact of the process. In this regard, a method of complex oxides synthesis in a medium of water vapor previously reported for several compositions [35,36] including $BaTiO_3$ [37–40] appears attractive as it is operated with widely available simple oxides as starting compounds and requires rather mild conditions for the reaction (temperature below 350 °C and autogenous vapor pressure). Compared to a technically relative hydrothermal method, this one doesn't imply the use of aggressive media of hardly removable auxiliary substances (NaOH, KOH). On the opposite to the hydrothermal reactions, which realize by the mechanism of the reactants' dissolution followed by homogenous nucleation and precipitation of the product [41–43], the synthesis of $BaTiO_3$ in water vapor was reported to occur *via* a solid-state transformation [39,40]. However, there is a lack of available detailed study of the mechanism for this transformation. Besides, the properties of ceramics from a $BaTiO_3$ powder synthesized in water vapor were poorly investigated as well as a technology for their production wasn't properly developed [38,39]. The current study was aimed to reveal the processes underlying $BaTiO_3$ formation from the simple oxides in a medium of water vapor and to perform a capability of the synthesized powder as a raw material for dielectric ceramics.

2. Results

2.1. Study of barium titanate formation in a water vapor medium

2.1.1. Composition of the reaction mixture

Conversion of an initial equimolar mixtures of BaO and TiO_2 in the rutile modification was observed during their isothermal dwell at 130 °C in vapor atmosphere with autogenous pressure of 0.27 MPa. The values of conversion calculated from the XRD patterns of the obtained products were shown in Table A1. After less than 100 minutes dwell, the obtained samples contained no $BaTiO_3$ phase according to XRD (samples NA-1…NA-6). Further changes in the composition of the initial oxide mixture performed an abrupt and non-monotonic character and had poor reproducibility. Introduction of some additives to the reaction mixture appeared to have a stabilizing effect on its transformation into $BaTiO_3$. Figure A1 showed the initial parts of kinetic curves reproducing $BaTiO_3$ formation from BaO and TiO_2 mixture with the addition of iodine as well as 1.2 wt. % of citric acid. Due to the presence of these additives, the observed part of the kinetic curves achieved a character of monotonic growth following the induction period, which took about 30 min. Table A2 presented the values of conversion corresponding to the mixtures of starting oxides with different amounts of citric acid, which have been treated in water vapor for equal time. Three-fold difference in the amounts of citric acid didn't have a significant effect on the degree of the reagents' conversion. For the further experiments on $BaTiO_3$ formation kinetics, 1.2 wt. % of citric acid were introduced to the reaction mixture.

2.1.2. Formal kinetic analysis of $BaTiO_3$ formation

Figure 1a demonstrated the degree of conversion in the initial mixture of BaO and TiO_2 versus the duration of its treatment in water vapor medium in the presence of citric acid. For each of the temperatures, there were two curves calculated based on the amounts of BaO and TiO_2 remained after the reaction, respectively. The kinetic curves possessed sigmoidal shape peculiar for the

 doi:10.20944/preprints202401.1870.v1

topochemical processes. When processed at 130 as well as at 140 °C, the reaction system passed the induction period, which was associated with the formation and spreading of the reaction zone. The kinetic curve corresponding to 150 °C contained no induction period, because it could occur during the heating. After about 150 min. of treatment at 150 °C, the conversion in the oxide mixture reached a plateau corresponding to 86 % of $BaTiO_3$ formed. Similarly, at 130 and 140 °C, the conversion of reagents didn't exceed 83-84 % with a plateau reached after 225 and 210 min. of the processing, respectively.

The analysis of the kinetic curves was provided using the Johnson-Mehl-Avrami-Erofeev equation, often applied for the processes in the solid state [44]:

$$\ln \ln \frac{1}{1-\alpha} = m\, lnk + m\, lnt, \qquad (1)$$

where α is the conversion, k is the rate constant, t is time, and m is a parameter. The results of the kinetic curves linearization were presented in Figure A2, while the calculated ln k and the parameter m were shown in Table 1.

Table 1. Kinetic parameters for $BaTiO_3$ formation in water vapor medium from the mixture of BaO and TiO_2 with addition of 1.2 wt.% of citric acid. The data calculated from the amounts of BaO ($BaCO_3$) and TiO_2 remained in the product.

Temperature (°C)	Parameters based on BaO amount		Parameters based on TiO_2 amount	
	m	ln k	m	ln k
130	1.59 ± 0.12	-5.11 ± 0.38	1.39 ± 0.14	-5.03 ± 0.50
140	1.52 ± 0.27	-4.71 ± 0.80	1.55 ± 0.32	-4.64 ± 0.91
150	1.01 ± 0.21	-3.98 ± 1.00	0.98 ± 0.17	-3.97 ± 0.64

According to Hancock and Sharp [45], some specific values of the parameter m could be used to determine the limiting stage of the solid-state reaction. Particularly, when m = 1.0…1.24, the reaction is limited by the processes occurring at the phase boundary. This could be applied to the considered reaction between BaO and TiO_2 at 150 °C as the parameter was about unity in that case. At lower temperatures, the approach by Hancock and Sharp wasn't applicable indicating that neither diffusion (m = 0.54…0.62) nor nucleation (m = 2.0…3.0) were the only limiting factors.

The Arrhenius plot was used to extract the apparent activation energy from the collected kinetic data (Figure 1b). Its values calculated based on the fractions of barium and titanium oxides remained in the mixture after each time of treatment were rather close and reached 74.8 and 79.6 kJ mol^{-1}, respectively.

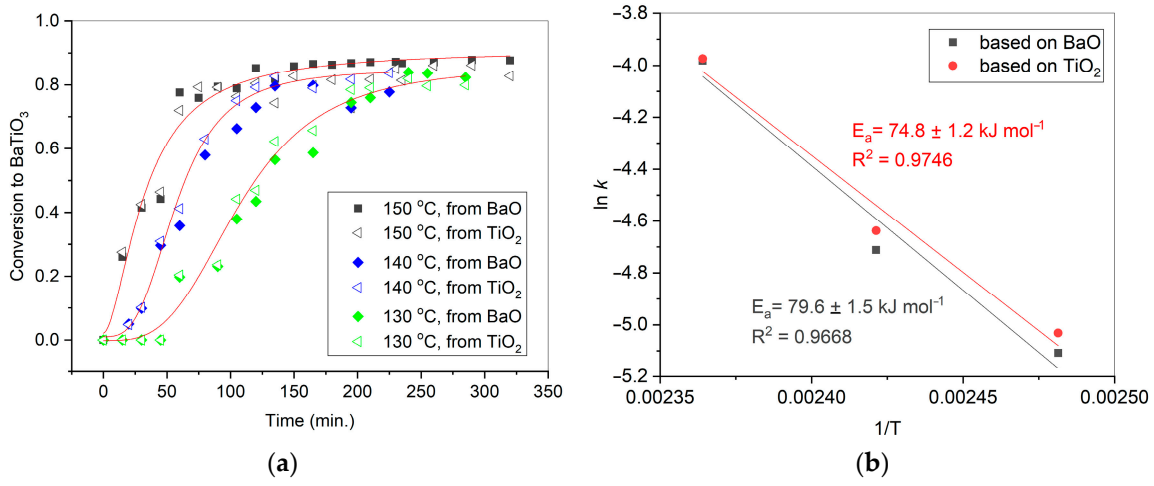

(**a**) (**b**)

Figure 1. Conversion of BaO and TiO_2 equimolar mixtures with 1.2 wt. % of citric acid in water vapor at 130-150 °C calculated from the amounts of $BaCO_3$ as well as TiO_2 in the products (**a**); Arrhenius plots derived from the kinetic curves (**b**).

 doi:10.20944/preprints202401.1870.v1

2.1.3. Microstructural study of $BaTiO_3$ formation

At the temperature of 130 °C, the reaction between BaO and TiO_2 in water vapor occurred the most slowly among the considered conditions, which allowed a detailed observation of $BaTiO_3$ formation by varying the time of treatment. In the sample obtained in 30 min. of processing and then drastically cooled, two main kinds of particle's shape were observed by the means of TEM (Figure 2a). Local EDX analysis (Figure 2b) revealed that rounded ones belonged to TiO_2 phase (probe II in Figure 2), while elongated particles contained Ba, C and O atoms among the detectable elements (probe I in Figure 2). XRD analysis of this sample showed that it consisted of $BaCO_3$ and TiO_2 in rutile modification (Figure 3). The presence of $BaCO_3$ could be explained as a result of the intensive interaction between Ba-containing species formed from BaO in water vapor and CO_2 from air, to which the sample was exposed after the synthesis and then stored before the analysis. Besides, there was a probe III which contained both types of metal ions (Ba, Ti) as well as oxygen and was likely to represent the early stage of $BaTiO_3$ formation. The composition of the studied sample corresponded to the termination of the induction period of the reaction (Figure 1a). Longer reaction time at 130 °C resulted in accumulation of the newly formed $BaTiO_3$ phase, which was observed in XRD patterns (Figure 3).

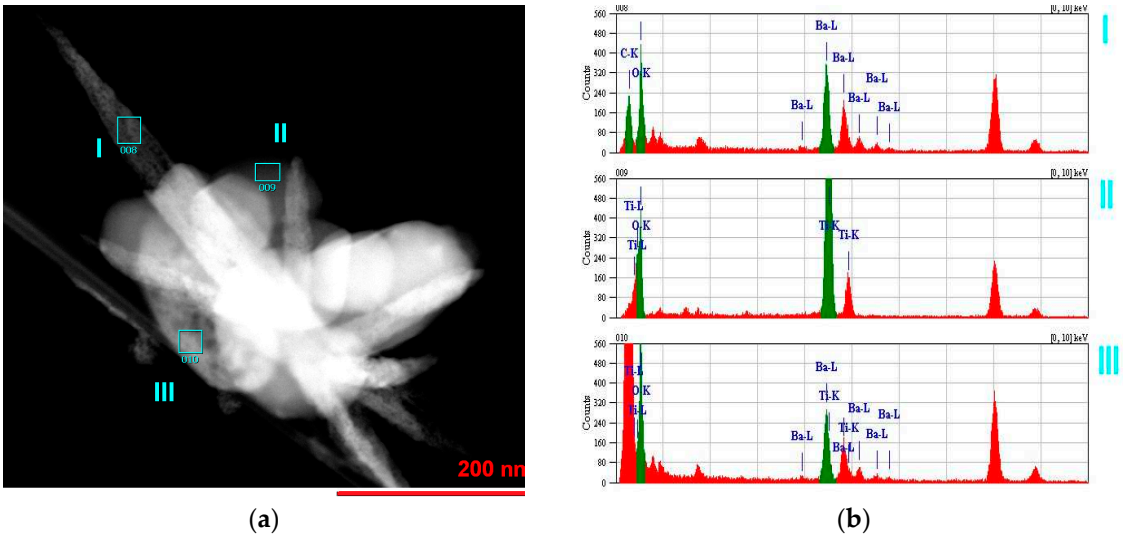

(**a**) (**b**)

Figure 2. TEM (**a**) and EDX (**b**) study of a sample prepared from BaO and TiO_2 equimolar mixtures with 1.2 wt. % of citric acid in water vapor at 130 °C for 30 min.

 doi:10.20944/preprints202401.1870.v1

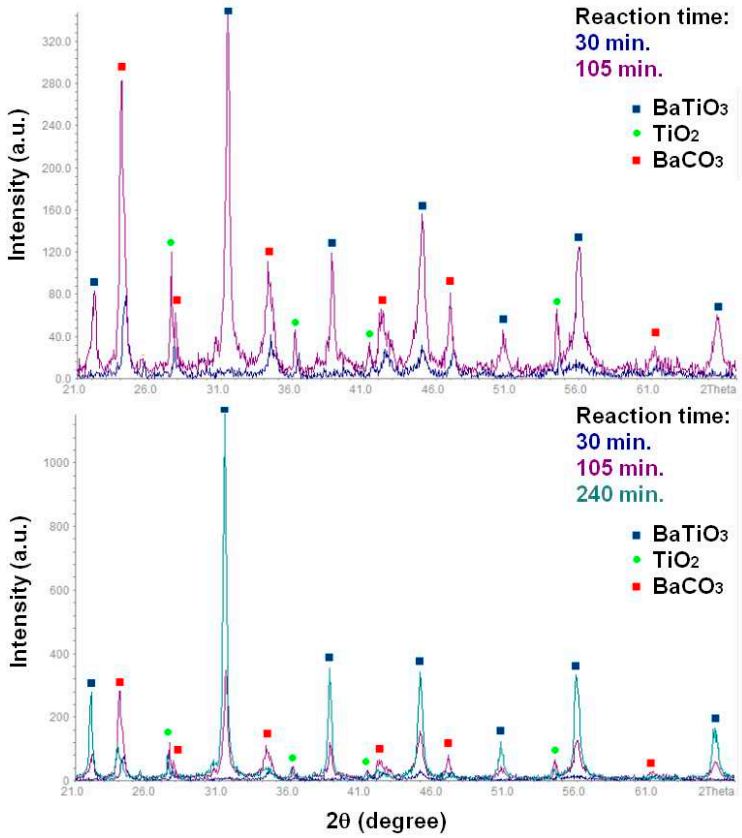

Figure 3. XDR patterns of the samples obtained from BaO and TiO_2 equimolar mixtures with 1.2 wt. % of citric acid in water vapor at 130 °C for 30-240 min.

Figure 4a showed the particles of TiO_2 contacting with the elongated particles of BaO derivative in the sample treated for 30 min. at 130 °C. Surface diffusion of the reagents led to formation of a neck between their particles. In this area indicated as a reaction zone in the Figure 4a, $BaTiO_3$ nucleation was expected to occur and to be followed by the formation of the product layer. Similar processes occurred in agglomerate shown in the bottom of Figure 4b, where one could see rounded TiO_2 crystals partially covered with a mass of another reagent. Also, in Figure 4b, it was clearly visible that elongated particles of Ba-containing reagent possessed a dendrite morphology, which pointed to their formation from a melt [46]. EDX analysis of the particles observed in Figure 4b was presented in Figure A3. The origin of the melt was probably connected to the initial BaO hydroxylation and hydration in water vapor followed by its melting. On drastic cooling of the reaction system, this melt solidified in the shape of dendrites. When contacted with air, the hydroxylated barium oxide formed $BaCO_3$, which was found by XRD and EDX. Another image of the found dendrite structures was shown in Figure A4.

 doi:10.20944/preprints202401.1870.v1

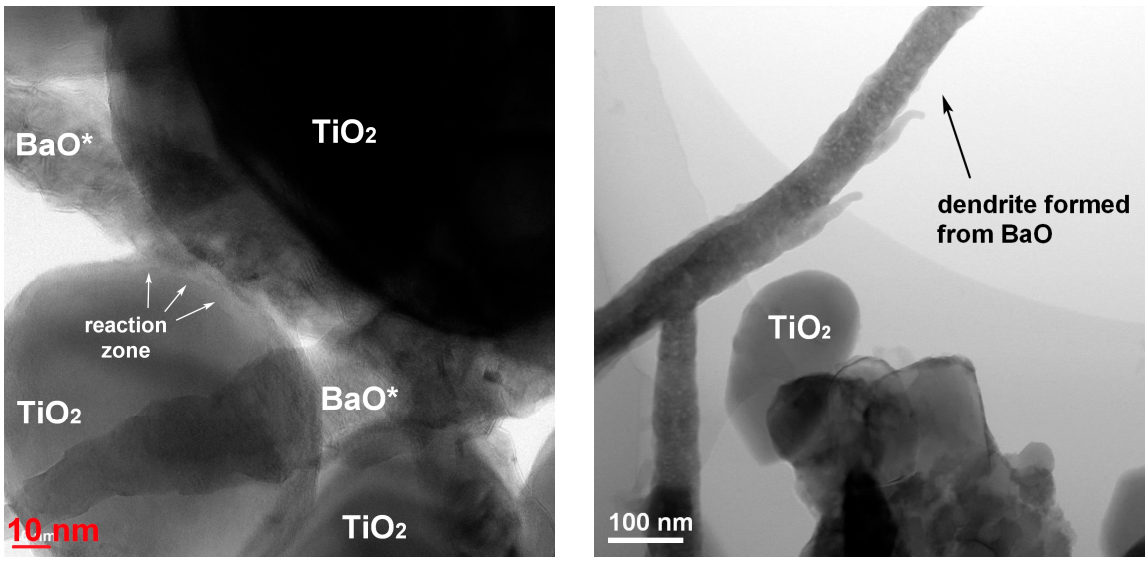

(**a**) (**b**)

Figure 4. HRTEM images (**a** and **b**) of the sample prepared from BaO and TiO_2 equimolar mixtures with 1.2 wt. % of citric acid in water vapor during 30 min. BaO* indicated the phase formed from initial BaO during the treatment in vapor and the following storage in air.

2.1.4. FTIR study of $BaTiO_3$ formation

Figures 5 performed fragments of FTIR spectra of the powders obtained at 130 °C by the treatment of BaO and TiO_2 equimolar mixture in vapor for 15…285 min. The whole spectra in a range of 4000…350 cm^{-1} were shown in Figure A5. Valence vibration bands of Ti-O and Ba-O bonds [37,47] were detected at about 400 and 500 cm^{-1} in every studied sample, but in the spectra corresponding to 15 and 30 min. of the treatment, the latter band was asymmetrically broadened towards higher wavenumbers. This band broadening pointed to a weakening of Ti-O-Ti bonds and matched with the induction period in the corresponding kinetic curve (Figure 1a). Further narrowing of the mentioned band during the treatment reflected saturation of titanium coordination sphere, which naturally accompanied the formation of a new phase of $BaTiO_3$. There were bands between 1100 and 900 cm^{-1} (1095, 1025, 948, and 928 cm^{-1}), which gradually appeared in the spectra corresponding to 30 to 285 min. of the treatment and might be considered as obertones of the structural vibration in a range of 600…350 cm^{-1}. On one hand, it pointed to the increase of metal-oxide bonding with the time spent on reactants conversion in $BaTiO_3$. But also, the multiplicity of these obertones highlighted and imperfect structure of the solid and the presence of similar bonds of different energies, which was attributed to the solid-state transformation.

Wide bands observed in a range of 3500…3400 cm^{-1} as well as narrower ones at 1753 and 1060 cm^{-1} were related to the presence of the adsorbed water molecules and structural hydroxyl groups [48]. Noticeably, the band detected at about 3400 cm^{-1} and originated from the OH-stretching vibrations in the samples treated for 15 and 30 min. changed its shape in those synthesized during 90 or 285 min. The mentioned band splitted into a broad one, which slightly moved to lower frequencies, and a sharper band at 3500 cm^{-1}. Such an evolution of FTIR spectrum performed an involvement of water in the reactants' transformation. Band splitting in the mentioned wavelength region was studied for metal oxides exposed to water vapor and was explained by a different nature of OH groups [49]. In particular, the sharp band performed the vibrations in hydroxyls connected with metal ions from the lattice, while the broad one corresponded to OH-groups formed by structural oxygen protonation. Resolution of the bands was found to depend on the morphology of the solid as well as on the nature of crystallographic planes the hydroxyls were bonded with. Currently observed transition from a single broad band to a splitted one pointed to the structural changes in the solid phase caused by the failure of the parent TiO_2 structure and the formation of new crystallographic planes of $BaTiO_3$.

 doi:10.20944/preprints202401.1870.v1

The spectra shown in Figures 5 and C3 demonstrated the presence of $BaCO_3$ in the studied samples by its characteristic bands found at 2445, 2361, 1415, 856, and 692 cm^{-1}.

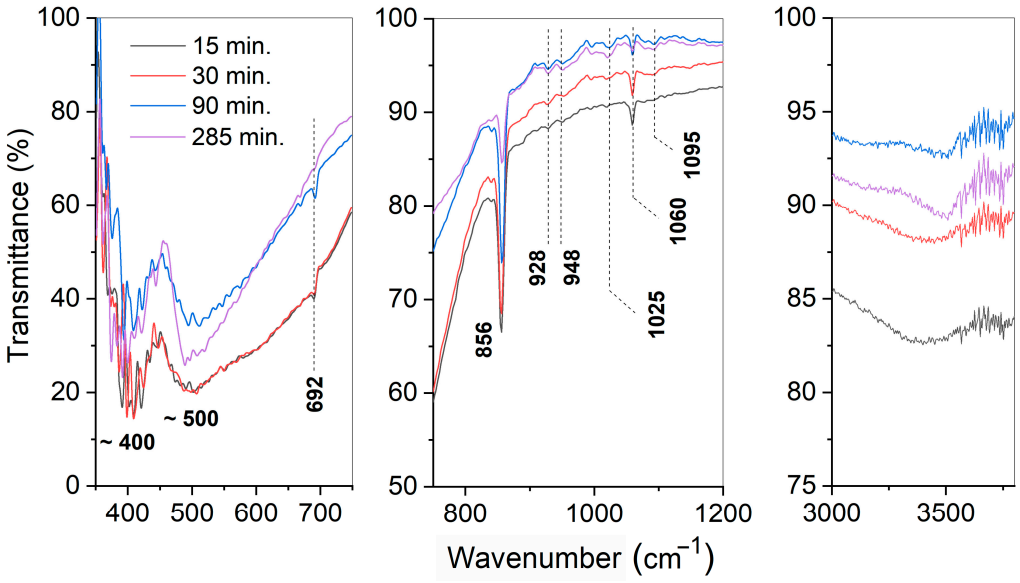

Figure 5. FTIR spectra of the samples prepared from BaO and TiO_2 equimolar mixtures with 1.2 wt. % of citric acid in water vapor using different time of treatment.

2.2. Properties of barium titanate ceramics sintered from the powder synthesized in water vapor medium

2.2.1. Characterization of the synthesized powder

In the kinetics and mechanism study of $BaTiO_3$ formation in water vapor at 130-150 °C described above, any single-phase powder wasn't obtained. A plateau at the $BaTiO_3$ formation curve corresponding to 150 °C was observed when the reagents' conversion approached to 86 %. This could be explained by diffusion limitations of both temperature and morphological nature. On one hand, the temperatures examined above might appear low for volume diffusion initiation, while surface diffusion couldn't support enough spreading of the reaction zone for the total reagents' transformation. On another hand, a growing product layer hindered the diffusion of reactants to the front of the reaction. Earlier, it was shown that the reaction in an equimolar BaO and TiO_2 mixture in vapor medium didn't finalize even after isothermal dwell at 230 °C for 20 h. [37]. However, when Ba/Ti molar ratio was increased to 1.10…1.14, a single-phase $BaTiO_3$ was successfully obtained [39,40]. In the current research, the reactants were provided by the same suppliers as in [37] and the conditions of treatment were repeated except to Ba/Ti molar ratio.

Figure 6a performed the results of XRD analysis of the samples synthesized from the initial oxide mixture by the treatment in vapor at 230 °C for 20 h. In accordance with [37], an equimolar mixture of the reactants led to the formation of $BaTiO_3$ with an admixture of TiO_2. Table 2 presented the calculated amounts of TiO_2 remained in the prepared powders. One could see that the increase of Ba/Ti ratio to 1.3 gradually carried to a full consumption of the initial TiO_2 and to the formation of a single-phase $BaTiO_3$ powder.

Preprints.org (www.preprints.org) | NOT PEER-REVIEWED | Posted: 26 January 2024 doi:10.20944/preprints202401.1870.v1

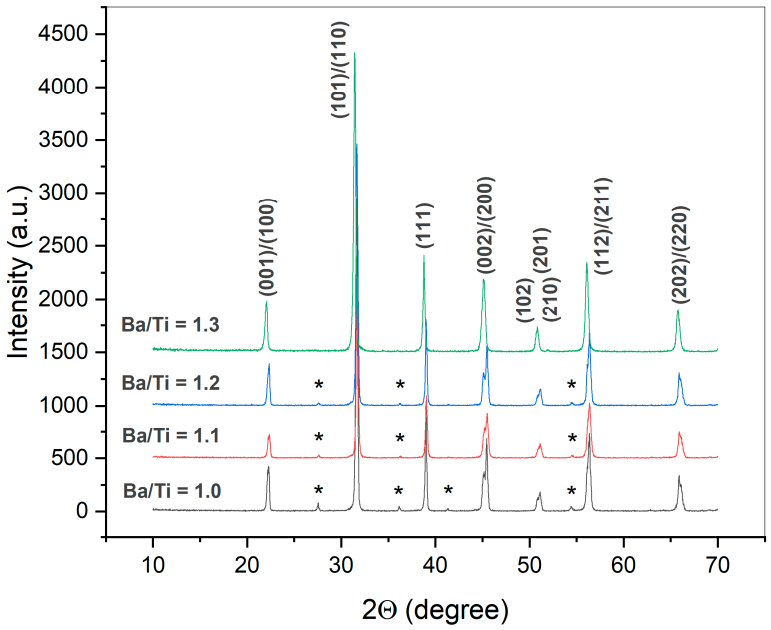

Figure 6. XRD patterns of the samples synthesized from BaO and TiO_2 mixtures with different Ba/Ti molar ratio in water vapor at 230 °C, 2.9 MPa for 20 h. The samples were preliminarily washed from the residual of Ba^{2+} ions. * indicated TiO_2 phase (rutile, PDF2 #021-1276). Miller indices corresponded to $BaTiO_3$ phase (PDF2 # 075-2117).

XRD patterns of the synthesized powders corresponded to $BaTiO_3$ in a tetragonal modification. A characteristic splitting of (002)/(200) peaks in the patterns were shown in Figure 6b. It was noticeable that the growth of barium excess in the reaction system resulted in a disappearance of this splitting. As it was calculated from the XRD data, the approaching of the reaction system to full transformation of TiO_2 into product was accompanied by a decrease in $BaTiO_3$ tetragonality (c/a cell parameter ratio) (Table 2). This could be connected to the formation of a core-shell structure of $BaTiO_3$ particles [50,51]. This phenomenon had been described for nanosized particles and grains of $BaTiO_3$. Previously [37], the particles obtained similarly to the current route were shown to consist of agglomerated crystals, which were 100-nm sized in average. Tetragonal phase known to be stable below the Curie point of $BaTiO_3$ (~ 130 °C) was reported to become deteriorated by a high concentration of structural defects near to the surface of the particle [52]. For this reason, it partially transforms into pseudocubic modification, which leads to a composite structure of the particle: a pseudocubic shell and a tetragonal core. Pseudocubic phase possesses the same XRD profile as a high-temperature cubic modification of $BaTiO_3$. Coexistence of the mentioned $BaTiO_3$ modifications and the changes in their fractions between the synthesized powders with different Ba/Ti ratio resulted in different tetragonality, which was calculated as an average value for each sample's volume.

Table 2. Residual TiO_2 amounts and tetragonality (c/a) in $BaTiO_3$ samples synthesized in water vapor at 230 °C and 2.94 MPa for 20 h with a different initial Ba/Ti molar ratio.

Ba/Ti ratio	TiO_2 amount (wt. %)	c/a
1.0	5.8	1.0073
1.1	4.1	1.0071
1.2	3.1	1.0068
1.3	0	1.0057

The morphologies of the initial TiO_2 powder and the resulting single-phase $BaTiO_3$ were shown in Figure 7. From the analysis of SEM images, $BaTiO_3$ powder consisted of micron-sized agglomerates of round-shaped particles from a range of 90 to 220 nm with a mean value of 135 nm (Figure 7b). The

 doi:10.20944/preprints202401.1870.v1

observed agglomerates were likely to form directly from the particles of TiO_2 (Figure 7a). Similar inheritance of the starting TiO_2 morphologies by $BaTiO_3$ during the synthesis in water vapor was described elsewhere [40]. Noticeably, the agglomerates visually differed in their density and neighbored to almost dispersed particles (Figure 7b). This pointed to a gradual deagglomeration of $BaTiO_3$ during the treatment in vapor, which should be accompanied naturally by an increase of the powder's surface area. Such an increase in surface could be considered as a factor governing the decrease of powder's tetragonality with approaching to the reaction termination (Table 2).

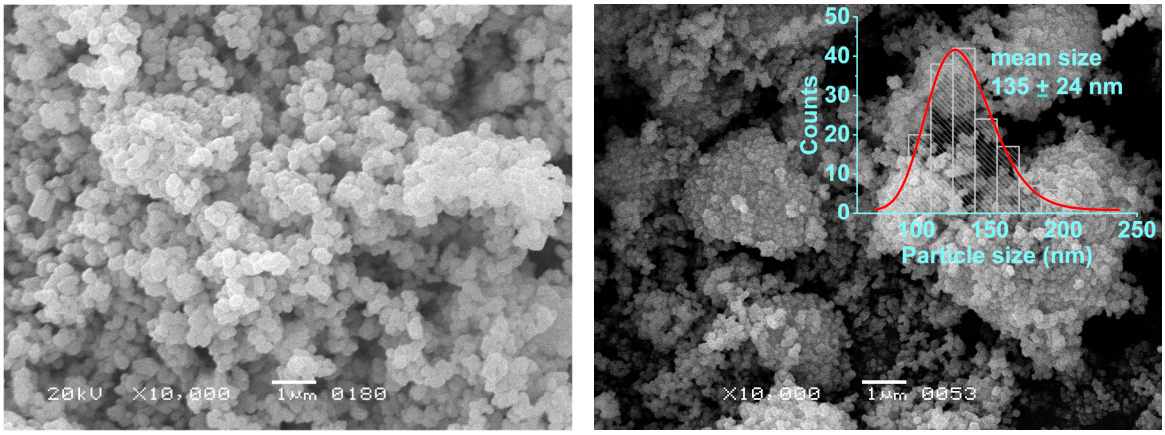

(**a**) (**b**)

Figure 7. This is SEM images of the initial TiO_2 powder (**a**) and $BaTiO_3$ synthesized from it in water vapor at 230 °C, 2.9 MPa during 20 h. with a molar ratio Ba/Ti = 1.3 in the reaction system.

The single-phase $BaTiO_3$ powder synthesized from BaO and TiO_2 mixture with Ba/Ti = 1.3 was selected as a raw material for ceramics manufacturing via conventional route including room-temperature pressing followed by a high-temperature sintering. To estimate its sintering behavior, a dilatometric analysis was provided (Figure 8). From 40 to 1025 °C, only thermal expansion with a constant rate was detected. In an interval of 1025-1080 °C, a fist stage of shrinkage associated with particles' re-orientation occurred and was followed by an interval of sintering accompanied by pore elimination. The highest rate of shrinkage was fount between 1252 and 1270 °C. Above 1295 °C, real sintering was expected to finalize and change to the grain growth.

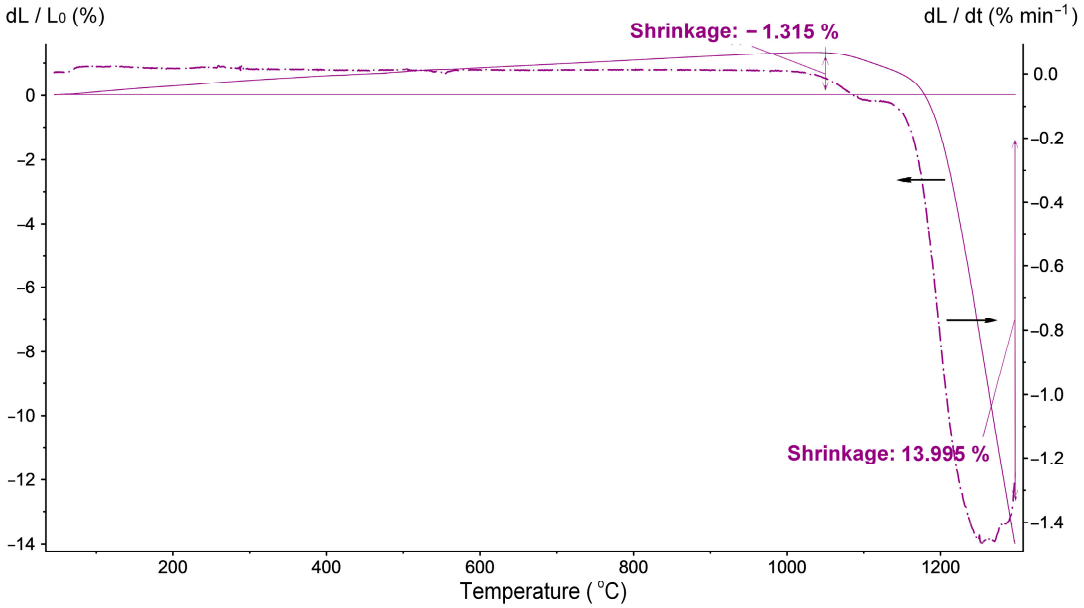

Figure 8. Shrinkage curve of $BaTiO_3$ powder synthesized from it in water vapor at 230 °C, 2.9 MPa during 20 h. with a molar ratio Ba/Ti = 1.3.

 doi:10.20944/preprints202401.1870.v1

2.2.2. Properties of the sintered ceramics

Starting from the results of the dilatometric investigation of the synthesized $BaTiO_3$ powder, its sintering was carried out in a temperature range of 1250…1350 °C. According to XRD analysis of the prepared ceramics, single-phase tetragonal $BaTiO_3$ was obtained at each of the sintering temperatures (Figure 9). Material consolidation and elimination of the structural defects during the ceramics processing relieved spontaneous polarization, which led to the tetragonality enhancement compared to the raw powder (c/a = 1.0057) (Table 3). Besides, the tetragonality slightly increased with the sintering temperature.

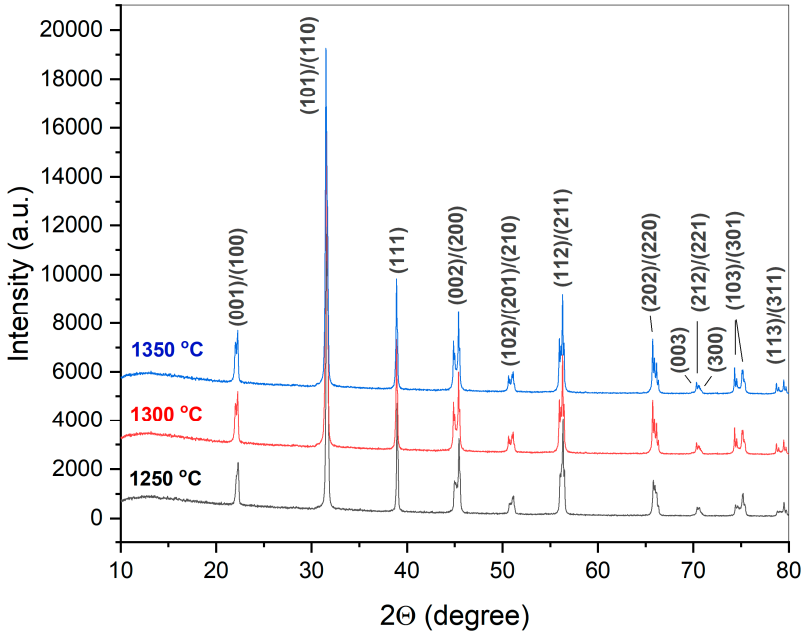

Figure 9. XRD patterns of crashed $BaTiO_3$ ceramics manufactured from the synthesized powder by uniaxial pressing at 150 MPa followed by 1-hour sintering at 1250 - 1350 °C. Miller indices indicated tetragonal $BaTiO_3$ modification.

SEM study of the prepared ceramics revealed a formation of rather dense microstructures (Figure 10). When sintered at 1250 °C, the material consisted of micron-sized grains (mean size 2.09 ± 0.44 μm) partially separated by open pore space (Figure 10a). Its relative density appeared 94 % (Table 3), which could be considered as high for the conventional ceramics technology. The material sintered at 1300 °C performed slightly higher density, but its microstructure was less homogenous demonstrating micron-grained areas (Figure 10b) neighboring to the regions with round-shaped pores (Figure 10c). The latter probably originated from discontinuous grain growth [53] in a fine-grained matrix. The presence of these large grains lowered the concentration of paraelectric grain boundaries [54,55] thus contributing to the increase in tetragonality. At 1350 °C, the sintering process occurred with an involvement of a liquid phase, which was reflected in the formation of large grains with spherical pores inside only (Figure 10c). Liqiud phase formation was caused by possible peritectoid and eutectoid processes, which were reported for nearly stoichiometric barium titanate compositions at 1250…1320 °C [56,57]. The relative density of the corresponding sample reached 96 %, and its tetragonality increased as well. However, the grain boundaries nearly disappeared, which together with the darkening of the sample proved the vicinity of the overburnt state.

 doi:10.20944/preprints202401.1870.v1

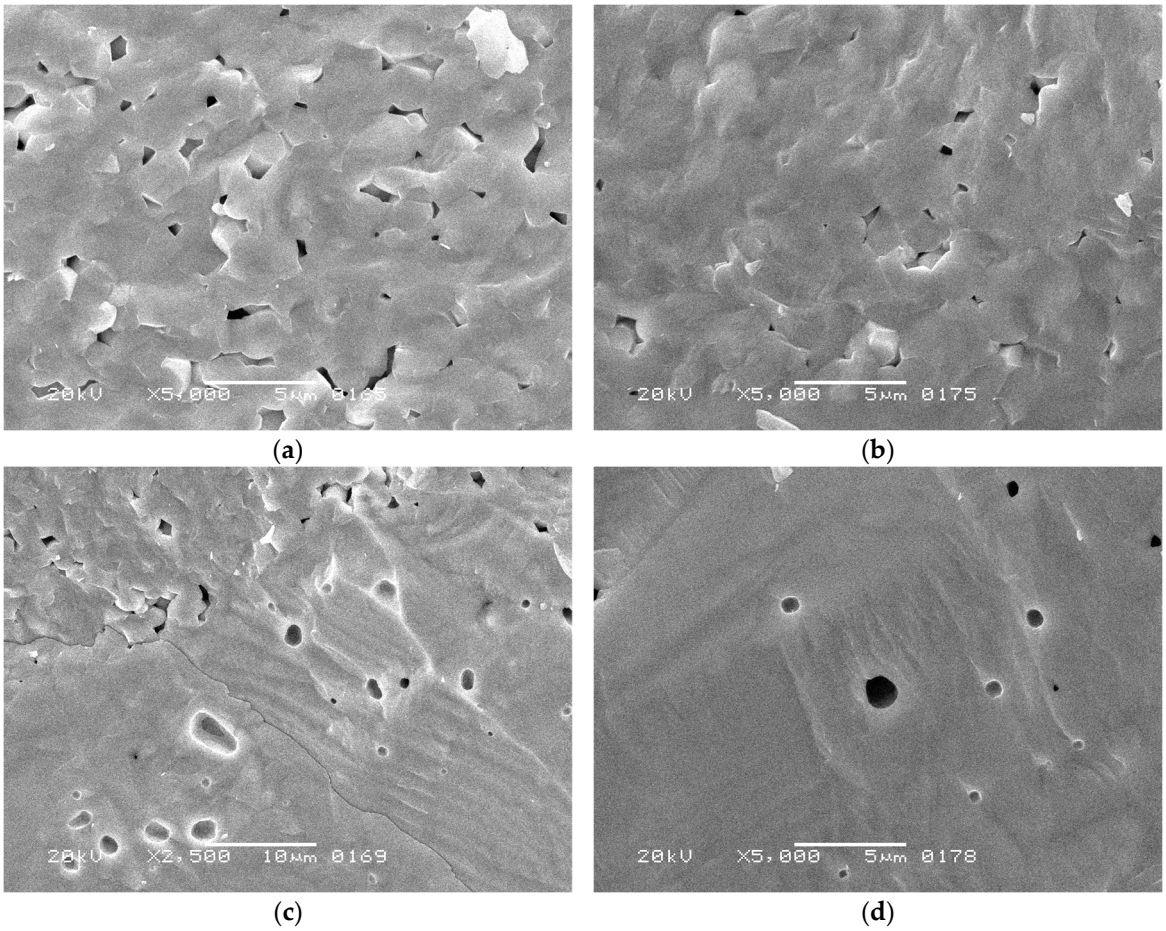

Figure 10. SEM images of fracture surfaces of $BaTiO_3$ ceramics manufactured from the synthesized powder by uniaxial pressing at 150 MPa followed by 1-hour sintering at: (a) 1250 °C; (b), (c) 1300 °C; (d) 1350 °C.

Despite the enhancement in the relative density and tetragonality of $BaTiO_3$ ceramics caused by the increase of the sintering temperature, their dielectric properties demonstrated high sensitivity to the microstructure (Table 3). The highest dielectric constant was determined for the fine-grained material sintered at 1250 °C. Structural inhomogeneities in the sample sintered at 1300 °C led to a comparative decrease in the permittivity, while approaching to a burnout at 1350 °C caused a drastic decrease of this characteristic. The loss tangent performed a sensitivity to the type of pore space. It was higher in the sample with open intergranular porosity (ceramics sintered a 1250 °C) then in those with combined inter- and intragranular pores (sintered a 1300 °C) or just closed porosity (sintered a 1350 °C). Open pores were prone to adsorb water molecules from the atmosphere, which caused extra conductivity.

Table 3. Structural and dielectric properties of the sintered $BaTiO_3$ ceramics.

Sintering temperature (°C)	Relative density (%)	Tetragonality c/a	Dielectric properties		
			Frequency	ε	tg δ 10^3
1250	94.3	1.0102	1 kHz	3879	6.7
			100 kHz	3761	10.0
			1 MHz	3720	23.0
1300	95.6	1.0106	1 kHz	3247	5.1
			100 kHz	3205	8.0
			1 MHz	3183	17.0
1350	96.0	1.0111	1 kHz	1822	5.3
			100 kHz	1794	4.1

 doi:10.20944/preprints202401.1870.v1

	1 MHz	1798	3.8

3. Discussion

Once subjected to water vapor, the particles of BaO and TiO_2 from the initial reaction mixture adsorbed water molecules and underwent surface hydroxylation. BaO is known to add water with the formation of a layer of amorphous hydroxide and further hydration into $Ba(OH)_2 \cdot xH_2O$ [58–60]. For TiO_2, both molecular and dissociative adsorption of water are typical [61]. Apparently, this resulted in formation of similar charges on the particle's surfaces, which led to their mutual repulsion. An introduction of foreign electrolyte locally changed the electrostatic conditions in the mixture and supported the formation of contacts between the reactants' particles. For this reason, the presence of small amounts of citric acid in the reaction mixture stabilized the initial stage of BaO and TiO_2 interaction. An additive of iodine reacted with water molecules to generate HI and HIO, which acted in a similar way as citric acid making for a stable growth of reagents' conversion with the time.

The observed reaction between the initial oxides possessed the features of a topochemical process [62]. The conversion *vs.* time curves for BaO-TiO_2 system in water vapor demonstrated sigmoidal shape with an induction period imprinted at 130 and 140 °C. At this stage, the reactants' hydration and hydroxylation occurred accompanied by melting of the hydrated $Ba(OH)_2$ as it was revealed by TEM. These processes allowed formation and growth of a contact area between the reactants' particles. Due to the interaction with water molecules, the surfaces of the reactants became highly defective, which facilitated the appearance of a reaction zone. $BaTiO_3$ nucleation and its growth initiated autolocalization of the process and moved the front of the reaction inward the TiO_2 particles. These autolocalization was accompanied and promoted by hydroxylation of the oxide structure as it was shown by FTIR study. The corresponding part of the kinetic curves performed an increase in $BaTiO_3$ fraction. From the analysis of kinetics, this complex process was likely to be controlled by the phase transformations rather than by diffusion. However, the collected data didn't allow any unambiguous conclusion whether the process was limited by the product nucleation or by the phase-boundary phenomena. Nevertheless, the final part of the kinetic curves, i.e. reaching a plateau, should be caused by the diffusion limitations, which were overcame by enough excess of barium ions in the reaction medium.

The calculated apparent activation energy of the studied reaction (75-80 kJ mol^{-1}) was close to those reported for $BaTiO_3$ formation from TiO_2 in a concentrated $Ba(OH)_2$ solution (105 kJ mol^{-1}) recognized as a topochemical process as well [63]. A conventional high-temperature solid-state synthesis of $BaTiO_3$ was characterized by a higher activation energy of 361 kJ mol^{-1}, while for a reaction between the same reactants ($BaCO_3$ and TiO_2) in water vapor at 700 °C it was determined as 142 kJ mol^{-1} [64]. These results emphasized a key role of water in facilitating the studied topochemical reaction due to defects generation on the surface of the reactants and further in their bulk. Current study proved the propositions and conclusions on the mechanism of $BaTiO_3$ formation from a mixture of simple oxides in water vapor outlined in the earlier works [37,39,40].

$BaTiO_3$ powder currently produced in water vapor performed rather high capability in the manufacturing of ceramics for low-frequency applications. Table 4 collected some of the recent data on the structural and dielectric characteristics of pure $BaTiO_3$ ceramics obtained by the conventional technique. Most of these materials were produced from nanosized or nearly nanosized powders by pressing at different loadings (50…400 Pa) with subsequent sintering at a temperature from a range of 1050…1350 °C for several hours. It is known that achievement of a full density is quite difficult for the conventional route, so the reported materials possessed relative densities of 92…97 % of the theoretical value (6.02 g cm^{-3}). However, the density is not the deciding factor for the functional properties of $BaTiO_3$ ceramics. In case of a sufficient densification, the grain size is known to affect the dielectric properties of $BaTiO_3$. Among them, the highest dielectric constant was observed when the grain size of $BaTiO_3$ was about 1 μm. This effect could be followed from the data in the Table 4 as well. The ceramics obtained in the current work performed worthy values of the dielectric constant compared to the other mentioned results. Besides, its loss tangent was maintained at the level of 0.02 up to 1 MHz, which was acceptable for this class of materials [65]. Nevertheless, the use of novel

 doi:10.20944/preprints202401.1870.v1

approaches different from the conventional ceramics manufacturing, for instance, two-step sintering [66–68], cold sintering process [69–72] etc., would open a perspective for microstructural engineering and effective application of $BaTiO_3$ powders synthesized in water vapor medium.

Table 4. Structural and dielectric properties of $BaTiO_3$ ceramics process by a conventional technique.

Ref.	Particle size	Ceramics processing parameters			Ceramics properties				f
		p (MPa)	T (°C)	Time (h)	GS** (μm)	ϱ_{rel}*** (%)	$\varepsilon^{\#}$	tg δ ##	
[73]	20…40 nm	n/a*	1350	3	0.5…2.0	97	1223	0.0035	1 MHz
[74]	2 μm	200	1250…1350	2	5	90	2200	n/a	5 MHz
	40 nm	200	1250…1350	2	1	95	5000	n/a	
[75]	150 nm	n/a	1050	4	n/a	95.5	2200	n/a	1 kHz
[76]	20 nm	100	1300	3	n/a	92	1700	n/a	1 kHz
[65]	137 nm	400	1250	1	0.3…2.0	95.8	4200	0.0370	10 kHz
[77]	100 nm	150	1100	6	2	95	3300	0.0700	1 kHz
[78]	n/a	n/a	1300	3	5.53	data	2000	~ 0.0300	1 k Hz
[79]	n/a	50	1350	2	1	n/a	3533	n/a	100 kHz
This work	135 nm	150	1250	1	2	94.3	3879	0.0067	1kHz
							3761	0.0100	100 kHz
							3720	0.0230	1 MHz

* n/a - not available; ** GS - mean grain size; ***ϱ_{rel} - relative density; $^{\#}\varepsilon$ - dielectric constant at room temperature; $^{\#\#}$tg δ - loss tangent at room temperature.

4. Materials and Methods

Barium oxide (BaO, purity > 99.9 %, GOST 10203-78, supplied by LLC Laverna-Lab, Moscow, Russia), titanium dioxide in a rutile modification (TiO_2, purity > 99.9 %, STP TU COMP 2-340-11 supplied by LLC Komponent-Reactiv, Moscow, Russia), citric acid monohydrate ($C_6H_8O_7 \cdot H_2O$, purity > 99.9 %, GOST 3652-69, supplied by JSC LenReactiv, St.-Petersburg, Russia) and crystalline iodine (I_2, purity > 98 %, GOST 4159-79, supplied by JSC LenReactiv, St.-Petersburg, Russia) were used as initial substances for the synthesis of $BaTiO_3$.

To prepare a reaction mixture, the calculated amounts of BaO and TiO_2 with Ba/Ti molar ratio of 1.0, 1.1, 1.2, or 1.3 were jointly mixed using an agate mortar and pestle and placed into PTFE containers. If it was provided, a corresponding amount of citric acid monohydrate (0.6; 1.2 or 2.4 wt. % with respect to the mixture) was added to the reactants and underwent the joint mixing. To introduce iodine additive to the reactants, it was preliminarily applied in the surface of TiO_2 as follows. An open crucible with 4 g of TiO_2 was placed into a glass buks containing 1 g of I_2. The buks was closed and stored at room temperature for 4 days. After that TiO_2 was removed and used for the preparation of a reaction mixture as it was described above. The PTFE container with the reaction mixture was placed into a laboratory stainless-steel autoclave of 12…17 cm^3 volume, which contained 2 ml of distilled water at the bottom. The autoclave was sealed and placed into a furnace to be heated up to 130…230 °C with a rate of 80 °C h^{-1}. The corresponding vapor pressure generated inside the autoclave was 0.27…2.94 MPa. The autoclave was stored in these conditions for 0 to 20 h, after which it was removed from the furnace and drastically cooled by dipping of its bottom in cold water (about 14 °C). This method of cooling allowed water to condense on the bottom inside the autoclave separately from the container with the product. After that, the autoclave was opened, the product was removed from it and dried in air at a temperature of 70…80 °C for 12 h. If it was provided, the product was washed in 5 wt. % acetic acid solution and distilled water to remove the excess of barium ions.

 doi:10.20944/preprints202401.1870.v1

Ceramics processing was carried out with the use of 5 wt. % of polyvinyl alcohol aqueous solution as a temporary binder. Green pellets were prepared by uniaxial pressing at 150 MPa and then sintered at 1250, 1300 or 1350 °C for 1 h in air. Density of the obtained ceramic samples was determined by Archimedes method using kerosene. The processing procedure as well as metallization were described in detail elsewhere [80].

XRD analysis of the synthesized powders and crashed ceramic samples was provided with the use of the following diffractometers: STOE STADI P with CuKα radiation (STOE & Cie GmbH, Darmstadt, Germany), Rigaku D/Max-2500 with CuKα radiation (Rigaku Corp. Tokyo, Japan), and PowDiX 600 with CuKα+β radiation (CJSC Linev Adani, Minsk, Belarus). The patterns were recorded in a range of $10° < 2\theta < 80°$ with a step of 0.02°. ICDD PDF2 database was used for the phase analysis [81]. Whole diffraction pattern profile fitting was carried out using Le Bail method by means of GSAS [82] and FullProf [83] software. The structural models of $BaTiO_3$ (tetragonal), TiO_2 (rutile) and $BaCO_3$ (witherite) were found in Crystallography Open Database [84]. Quantitative analysis of the samples as well as cell parameters refinement was provided by Rietveld method [85].

Scanning electron microscopy of the powders and the ceramics fracture surfaces was performed at Jeol JSM 6380 (Jeol Ltd., Tokyo, Japan). Transmission electron microscopy combined with EDX study was conducted using Jeol JEM-2100 F (Jeol Ltd., Tokyo, Japan).

FTIR study of the synthesized powders was provided at WQF-530A spectrometer (Beijing Beifen-Ruili Analytical Instrument (Group) Co. LTD, Beijing, China) in a wavenumber range of 4000…350 cm^{-1} by attenuated total reflectance method.

Dielectric constant and loss tangent of the sintered ceramic disks with metallized plane parallel sides were calculated from the capacitance measurements carried out at GW Instek LCR-78210 meter (Good Will Instrument Co., Ltd., Xinbei, Taiwan).

5. Conclusions

Currently, we have studied in detail the process of $BaTiO_3$ formation from a mixture of solid oxides of barium and titanium in a medium of water vapor being in equilibrium with the liquid at 130…230 °C and 0.27…2.94 MPa. This process was revealed to occur as a topochemical reaction, which could be divided in an induction period and the following periods of a rapid conversion and its deceleration. The initial reactants underwent first surface hydration and further hydroxylation, which facilitated the autolocalization of the process. Barium oxide was found to transform into a melt when exposed to the conditions of the synthesis in water vapor. The apparent activation energy of $BaTiO_3$ formation in water vapor was estimated as 75…79 kJ mol^{-1}. To obtain a single-phase $BaTiO_3$ in these conditions, an excess of barium ions was required corresponding to Ba/Ti molar ratio equal to 1.3 in the initial mixture. At 230 °C and a vapor pressure of 2.94 MPa, a tetragonal $BaTiO_3$ powder with a mean particle size of 135 ± 44 nm was obtained. Based on this powder, a conventional ceramics technique allowed preparation of single-phase tetragonal $BaTiO_3$ ceramics with a grain size of about 2 μm and a room-temperature dielectric constant of 3820…3791 depending on the frequency and a loss tangent less than 0.02. Synthesis of $BaTiO_3$ in water vapor was proved as an effective and environmentally benign route to high-performance dielectric ceramics.

Author Contributions: Conceptualization, A.A.K., Y.D.I., M.N.D., and Y.Y.; methodology, A.A.K., Y.D.I., M.N.D., and A.V.S.; validation, A.A.K., Y.D.I. and M.N.D.; formal analysis, A.A.K, A.N.K., and L.A.A.; investigation, A.A.K., G.P.M., A.V.E., A.D.S., A.N.K., L.A.A., and V.E.B.; resources, M.N.D. and A.A.S.; data curation, A.A.K.; writing—original draft preparation, A.A.K.; writing—review and editing, A.V.S.; visualization, A..,K.; supervision, Y.D.I., M.N.D., and A.V.S.; project administration, A.V.S.; funding acquisition, A.V.S. All authors have read and agreed to the published version of the manuscript.

Funding: The article was written as part of the implementation of indicators for projects funded from the state budget or other external sources: the National Project "Science and Universities" to achieve the result "Creation of new laboratories, including under the guidance of young promising researchers (growing result)." FSFZ-2022-0003.

Data Availability Statement: The research data is available upon a request.

 doi:10.20944/preprints202401.1870.v1

Acknowledgments: The study was supported in part by Lomonosov Moscow State University Program of Development. The authors are thankful to Dr. Nellya A. Popova from Mendeleev University of Chemical Technology of Russia for her kind assistance in the dilatometric study.

Conflicts of Interest: The authors declare no conflicts of interest.

Appendix A

Table A1. Conversion of the equimolar mixture of BaO and TiO_2 after being exposed to vapor at 130 °C, 0.27 MPa for different time.

Sample	Exposition (min.)	Conversion to $BaTiO_3$ (%)
NA-1	0	0
NA-2	10	0
NA-3	20	0
NA-4	30	0
NA-5	40	0
NA-6	100	0
NA-7		73.5
NA-8	110	0
NA-9		42.8
NA-10		77.6
NA-11	120	75.7
NA-12		15.3
NA-13		70.7
NA-14	130	0
NA-15		53.6
NA-16	140	25.6
NA-17	150	29.0
NA-18	160	65.7
NA-19	170	83.5
NA-20	180	0

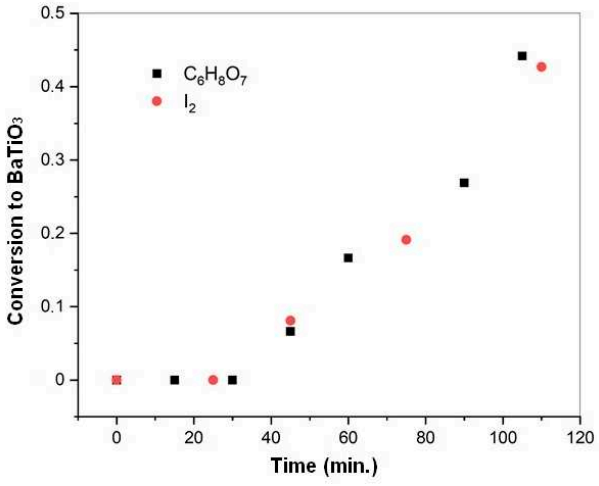

Figure A1. Conversion of the equimolar mixture of BaO and TiO_2 with the additive of iodine and 1.2 wt. % of citric acid in water vapor at 130 °C and 0.27 MPa.

Table A2. Conversion of the equimolar mixture of BaO and TiO_2 with the additive of citric acid after the treatment in water vapor at 130 130 °C and 0.27 MPa for 105 min.

Sample	Amount of citric acid (wt. %)	Conversion to $BaTiO_3$ (%)
CA-8	0.6	42.9

 doi:10.20944/preprints202401.1870.v1

CA-9	1.2	44.2
CA-10	2.4	45.0

Appendix B

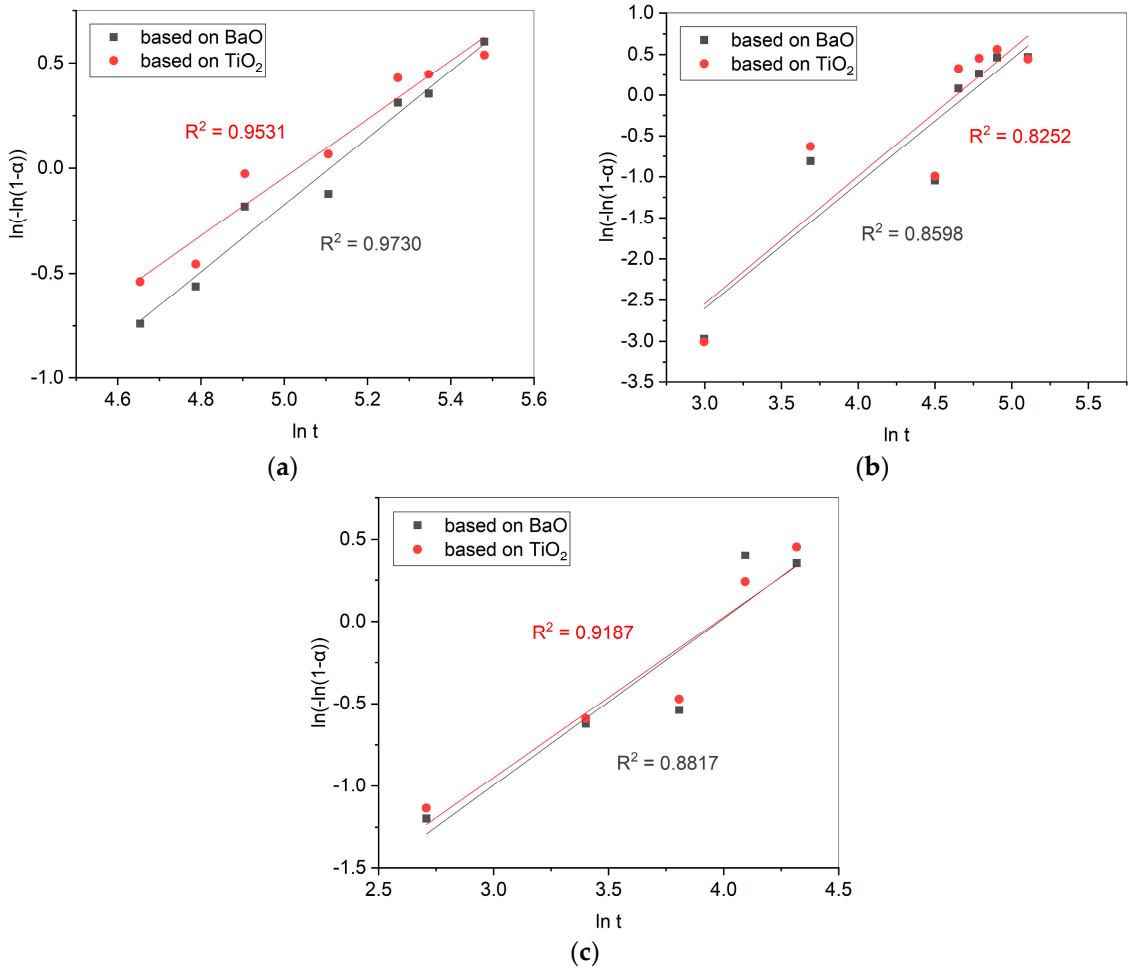

Figure A2. Johnson-Mehl-Avrami-Erofeev linearization of the kinetic curves of BaTiO3 formation in water vapor medium at different temperatures: (**a**) 130 °C; (**b**) 140 °C; (**c**) 150 °C. The data were obtained from the amounts of unreacted BaO and TiO_2 for each time of the reaction.

 doi:10.20944/preprints202401.1870.v1

Appendix C

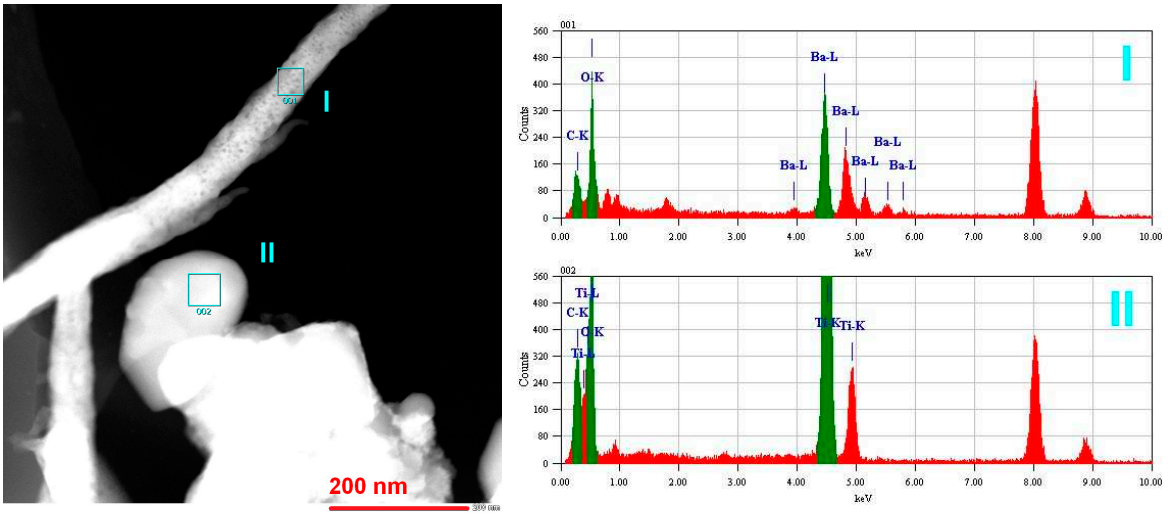

(**a**) (**b**)

Figure A3. TEM (**a**) and EDX (**b**) analysis of a sample prepared from BaO and TiO_2 equimolar mixtures with 1.2 wt. % of citric acid in water vapor at 130 °C for 30 min.

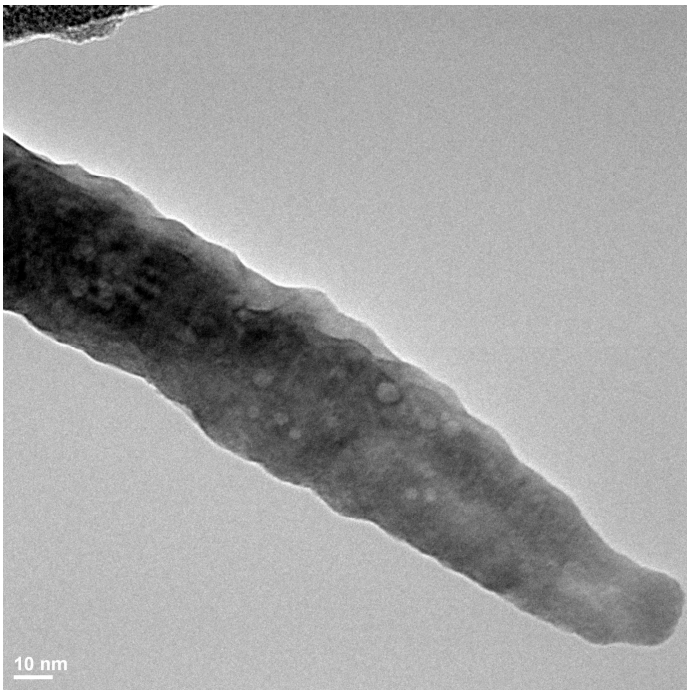

Figure A4. TEM image of a dendrite structure found in a sample prepared from BaO and TiO_2 equimolar mixtures with 1.2 wt. % of citric acid in water vapor at 130 °C for 30 min.

 doi:10.20944/preprints202401.1870.v1

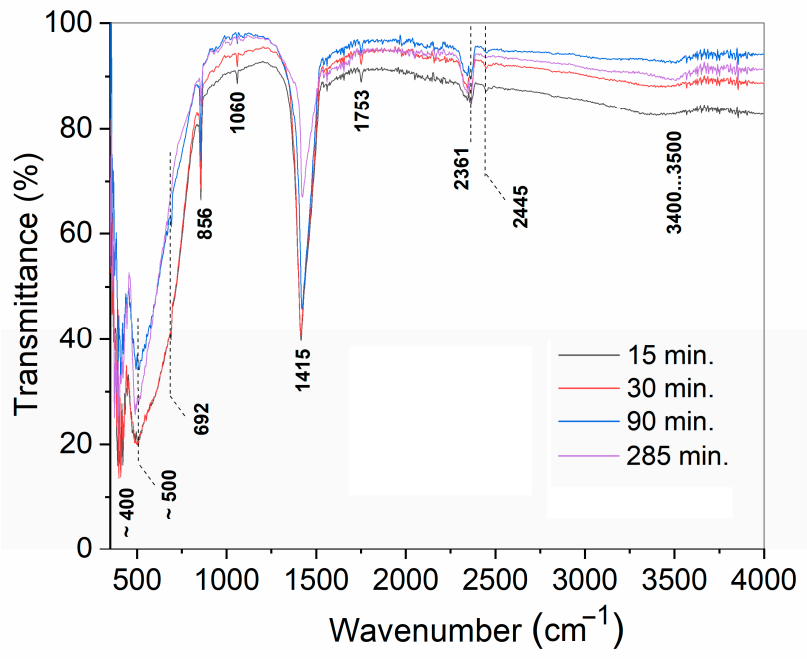

Figure A5. FTIR spectra of the samples prepared from BaO and TiO_2 equimolar mixtures with 1.2 wt. % of citric acid in water vapor using different time of treatment.

References

1. Zhao, C.; Wu, H.; Li, F.; Cai, Y.; Zhang, Y.; Song, D.; Wu, J.; Lyu, X.; Yin, J.; Xiao, D.; et al. Practical High Piezoelectricity in Barium Titanate Ceramics Utilizing Multiphase Convergence with Broad Structural Flexibility. *J. Am. Chem. Soc.* **2018**, *140*, 15252–15260. https://doi.org/10.1021/jacs.8b07844.
2. Sufiiarov, V.; Kantyukov, A.; Popovich, A.; Sotov, A. Structure and Properties of Barium Titanate Lead-Free Piezoceramic Manufactured by Binder Jetting Process. *Materials* **2021**, *14*, 4419. https://doi.org/10.3390/ma14164419.
3. Schipf, D.R.; Yesner, G.H.; Sotelo, L.; Brown, C.; Guild, M.D. Barium Titanate 3–3 Piezoelectric Composites Fabricated Using Binder Jet Printing. *Additive Manufacturing* **2022**, *55*, 102804. https://doi.org/10.1016/j.addma.2022.102804.
4. Li, M.; Jiang, B.; Cao, S.; Song, X.; Zhang, Y.; Huang, L.; Yuan, Q. Flexible Cellulose-Based Piezoelectric Composite Membrane Involving PVDF and $BaTiO_3$ Synthesized with the Assistance of TEMPO-Oxidized Cellulose Nanofibrils. *RSC Adv.* **2023**, *13*, 10204–10214. https://doi.org/10.1039/D3RA00604B.
5. Cao, Y.; Tan, S.L.; Cheung, E.J.H.; Siew, S.Y.; Li, C.; Liu, Y.; Tang, C.S.; Lal, M.; Chen, G.; Dogheche, K.; et al. A Barium Titanate-on-Oxide Insulator Optoelectronics Platform. *Advanced Materials* **2021**, *33*, 2101128. https://doi.org/10.1002/adma.202101128.
6. Bell, J.G.; Graule, T.; Stuer, M. Barium Titanate-Based Thermistors: Past Achievements, State of the Art, and Future Perspectives. *Applied Physics Reviews* **2021**, *8*, 031318. https://doi.org/10.1063/5.0048697.
7. Guo, X. Insulator-to-Semiconductor Transition of Nanocrystalline $BaTiO_3$ at Temperatures ≤ 200 °C. *Phys. Chem. Chem. Phys.* **2014**, *16*, 20420–20423. https://doi.org/10.1039/C4CP01914H.
8. Damamme, R.; Seveyrat, L.; Borta-Boyon, A.; Nguyen, V.-C.; Le, M.-Q.; Cottinet, P.-J. 3D Printing of Doped Barium-Titanate Using Robocasting - Toward New Generation Lead-Free Piezoceramic Transducers. *Journal of the European Ceramic Society* **2023**, *43*, 3297–3306. https://doi.org/10.1016/j.jeurceramsoc.2023.02.054.
9. Sydorchuk, V.; Khalameida, S.; Skwarek, E.; Biedrzycka, A. Some Applications of Barium Titanate Prepared by Different Methods. *Physicochem. Probl. Miner. Process.* **2022**. https://doi.org/10.37190/ppmp/147192.
10. Panthi, G.; Park, M. Approaches for Enhancing the Photocatalytic Activities of Barium Titanate: A Review. *Journal of Energy Chemistry* **2022**, *73*, 160–188. https://doi.org/10.1016/j.jechem.2022.06.023.

11. Poon, K.K.; Schafföner, S.; Einarsrud, M.-A.; Glaum, J. Barium Titanate-Based Bilayer Functional Coatings on Ti Alloy Biomedical Implants. *Journal of the European Ceramic Society* **2021**, *41*, 2918–2922. https://doi.org/10.1016/j.jeurceramsoc.2020.12.023.
12. Fakhar-e-Alam, M.; Saddique, S.; Hossain, N.; Shahzad, A.; Ullah, I.; Sohail, A.; Khan, M.J.I.; Saadullah, M. Synthesis, Characterization, and Application of $BaTiO_3$ Nanoparticles for Anti-Cancer Activity. *J Clust Sci* **2023**, *34*, 1745–1755. https://doi.org/10.1007/s10876-022-02346-y.
13. Sood, A.; Desseigne, M.; Dev, A.; Maurizi, L.; Kumar, A.; Millot, N.; Han, S.S. A Comprehensive Review on Barium Titanate Nanoparticles as a Persuasive Piezoelectric Material for Biomedical Applications: Prospects and Challenges. *Small* **2023**, *19*, 2206401. https://doi.org/10.1002/smll.202206401.
14. Potnis, P.; Tsou, N.-T.; Huber, J. A Review of Domain Modelling and Domain Imaging Techniques in Ferroelectric Crystals. *Materials* **2011**, *4*, 417–447. https://doi.org/10.3390/ma4020417.
15. Yang, X.; Li, D.; Ren, Z.H.; Zeng, R.G.; Gong, S.Y.; Zhou, D.K.; Tian, H.; Li, J.X.; Xu, G.; Shen, Z.J.; et al. Colossal Dielectric Performance of Pure Barium Titanate Ceramics Consolidated by Spark Plasma Sintering. *RSC Adv.* **2016**, *6*, 75422–75429. https://doi.org/10.1039/C6RA14741K.
16. Pithan, C.; Hennings, D.; Waser, R. Progress in the Synthesis of Nanocrystalline $BaTiO_3$ Powders for MLCC. *Int J Applied Ceramic Tech* **2005**, *2*, 1–14. https://doi.org/10.1111/j.1744-7402.2005.02008.x.
17. Yoon, D.-H. Tetragonality of Barium Titanate Powder for a Ceramic Capacitor Application. *J Ceram Proc Res* **2006**, *7*, 343–354.
18. Buscaglia, M.T.; Bassoli, M.; Buscaglia, V.; Alessio, R. Solid-State Synthesis of Ultrafine $BaTiO_3$ Powders from Nanocrystalline $BaCO_3$ and TiO_2. *Journal of the American Ceramic Society* **2005**, *88*, 2374–2379. https://doi.org/10.1111/j.1551-2916.2005.00451.x.
19. Brzozowski, E.; Castro, M.S. Synthesis of Barium Titanate Improved by Modifications in the Kinetics of the Solid State Reaction. *Journal of the European Ceramic Society* **2000**, *20*, 2347–2351. https://doi.org/10.1016/S0955-2219(00)00148-5.
20. Roy, A.C.; Mohanta, D. Structural and Ferroelectric Properties of Solid-State Derived Carbonate-Free Barium Titanate ($BaTiO_3$) Nanoscale Particles. *Scripta Materialia* **2009**, *61*, 891–894. https://doi.org/10.1016/j.scriptamat.2009.07.022.
21. Stojanovic, B.D.; Simoes, A.Z.; Paiva-Santos, C.O.; Jovalekic, C.; Mitic, V.V.; Varela, J.A. Mechanochemical Synthesis of Barium Titanate. *Journal of the European Ceramic Society* **2005**, *25*, 1985–1989. https://doi.org/10.1016/j.jeurceramsoc.2005.03.003.
22. Kong, L.B.; Zhang, T.S.; Ma, J.; Boey, F. Progress in Synthesis of Ferroelectric Ceramic Materials via High-Energy Mechanochemical Technique. *Progress in Materials Science* **2008**, *53*, 207–322. https://doi.org/10.1016/j.pmatsci.2007.05.001.
23. Sundararajan, T.; Prabu, S.B.; Vidyavathy, S.M. Combined Effects of Milling and Calcination Methods on the Characteristics of Nanocrystalline Barium Titanate. *Materials Research Bulletin* **2012**, *47*, 1448–1454. https://doi.org/10.1016/j.materresbull.2012.02.044.
24. Ramajo, L.; Parra, R.; Reboredo, M.; Zaghete, M.; Castro, M. Heating Rate and Temperature Effects on the $BaTiO_3$ Formation by Thermal Decomposition of (Ba,Ti) Organic Precursors during the Pechini Process. *Materials Chemistry and Physics* **2008**, *107*, 110–114. https://doi.org/10.1016/j.matchemphys.2007.06.050.
25. Duran, P.; Gutierrez, D.; Tartaj, J.; Moure, C. Densification Behaviour, Microstructure Development and Dielectric Properties of Pure $BaTiO_3$ Prepared by Thermal Decomposition of (Ba,Ti)-Citrate Polyester Resins. *Ceramics International* **2002**, *28*, 283–292. https://doi.org/10.1016/S0272-8842(01)00092-X.
26. Wada, S.; Kondo, S.; Moriyoshi, C.; Kuroiwa, Y. Preparation of Highly Dispersed Barium Titanate Nanoparticles from Barium Titanyl Oxalate Nanoparticles and Their Dielectric Properties. *jjap* **2008**, *47*, 7612. https://doi.org/10.1143/JJAP.47.7612.
27. Peng, Z.; Chen, Y. Preparation of $BaTiO_3$ Nanoparticles in Aqueous Solutions. *Microelectronic Engineering* **2003**, *66*, 102–106. https://doi.org/10.1016/S0167-9317(03)00032-7.
28. Jung, D.S.; Hong, S.K.; Cho, J.S.; Kang, Y.C. Nano-Sized Barium Titanate Powders with Tetragonal Crystal Structure Prepared by Flame Spray Pyrolysis. *Journal of the European Ceramic Society* **2008**, *28*, 109–115. https://doi.org/10.1016/j.jeurceramsoc.2007.05.018.
29. Testino, A.; Buscaglia, M.T.; Buscaglia, V.; Viviani, M.; Bottino, C.; Nanni, P. Kinetics and Mechanism of Aqueous Chemical Synthesis of $BaTiO_3$ Particles. *Chem. Mater.* **2004**, *16*, 1536–1543. https://doi.org/10.1021/cm031130k.

30. Viviani, M.; Buscaglia, M.T.; Testino, A.; Buscaglia, V.; Bowen, P.; Nanni, P. The Influence of Concentration on the Formation of $BaTiO_3$ by Direct Reaction of $TiCl_4$ with $Ba(OH)_2$ in Aqueous Solution. *Journal of the European Ceramic Society* **2003**, *23*, 1383–1390. https://doi.org/10.1016/S0955-2219(02)00357-6.
31. Ianculescu, A.C.; Vasilescu, C.A.; Crisan, M.; Raileanu, M.; Vasile, B.S.; Calugaru, M.; Crisan, D.; Dragan, N.; Curecheriu, L.; Mitoseriu, L. Formation Mechanism and Characteristics of Lanthanum-Doped $BaTiO_3$ Powders and Ceramics Prepared by the Sol–Gel Process. *Materials Characterization* **2015**, *106*, 195–207. https://doi.org/10.1016/j.matchar.2015.05.022.
32. Boulos, M.; Guillemetfritsch, S.; Mathieu, F.; Durand, B.; Lebey, T.; Bley, V. Hydrothermal Synthesis of Nanosized $BaTiO_3$ Powders and Dielectric Properties of Corresponding Ceramics. *Solid State Ionics* **2005**, *176*, 1301–1309. https://doi.org/10.1016/j.ssi.2005.02.024.
33. Ávila, H.A.; Ramajo, L.A.; Reboredo, M.M.; Castro, M.S.; Parra, R. Hydrothermal Synthesis of $BaTiO_3$ from Different Ti-Precursors and Microstructural and Electrical Properties of Sintered Samples with Submicrometric Grain Size. *Ceramics International* **2011**, *37*, 2383–2390. https://doi.org/10.1016/j.ceramint.2011.03.032.
34. Cai, W.; Rao, T.; Wang, A.; Hu, J.; Wang, J.; Zhong, J.; Xiang, W. A Simple and Controllable Hydrothermal Route for the Synthesis of Monodispersed Cube-like Barium Titanate Nanocrystals. *Ceramics International* **2015**, *41*, 4514–4522. https://doi.org/10.1016/j.ceramint.2014.11.146.
35. Danchevskaya, M.N.; Ivakin, Yu.D.; Torbin, S.N.; Muravieva, G.P.; Ovchinnikova, O.G. Thermovaporous Synthesis of Complicated Oxides. *J Mater Sci* **2006**, *41*, 1385–1390. https://doi.org/10.1007/s10853-006-7411-0.
36. Ivakin, Yu.D.; Danchevskaya, M.N.; Ovchinnikova, O.G.; Muravieva, G.P. Thermovaporous Synthesis of Fine Crystalline Gahnite ($ZnAl_2O_4$). *J Mater Sci* **2006**, *41*, 1377–1383. https://doi.org/10.1007/s10853-006-7410-1.
37. Kholodkova, A.A.; Danchevskaya, M.N.; Ivakin, Y.D.; Muravieva, G.P.; Tyablikov, A.S. Crystalline Barium Titanate Synthesized in Sub- and Supercritical Water. *The Journal of Supercritical Fluids* **2016**, *117*, 194–202. https://doi.org/10.1016/j.supflu.2016.06.018.
38. Kholodkova, A.; Danchevskaya, M.; Popova, N. Preparation and Dielectric Properties of Thermo-Vaporous $BaTiO_3$ Ceramics. *Mater. Tehnol.* **2015**, *49*, 447–451. https://doi.org/10.17222/mit.2013.276.
39. Kholodkova, A.A.; Danchevskaya, M.N.; Ivakin, Yu.D.; Muravieva, G.P. Synthesis of Fine-Crystalline Tetragonal Barium Titanate in Low-Density Water Fluid. *The Journal of Supercritical Fluids* **2015**, *105*, 201–208. https://doi.org/10.1016/j.supflu.2015.05.004.
40. Kholodkova, A.A.; Danchevskaya, M.N.; Ivakin, Yu.D.; Muravieva, G.P.; Ponomarev, S.G. Effect of Reagents on the Properties of Barium Titanate Synthesized in Subcritical Water. *Russ. J. Phys. Chem. B* **2018**, *12*, 1261–1268. https://doi.org/10.1134/S1990793118080079.
41. Eckert, J.O.; Hung-Houston, C.C.; Gersten, B.L.; Lencka, M.M.; Riman, R.E. Kinetics and Mechanisms of Hydrothermal Synthesis of Barium Titanate. *Journal of the American Ceramic Society* **1996**, *79*, 2929–2939. https://doi.org/10.1111/j.1151-2916.1996.tb08728.x.
42. Pinceloup, P.; Courtois, C.; Vicens, J.; Leriche, A.; Thierry, B. Evidence of a Dissolution–Precipitation Mechanism in Hydrothermal Synthesis of Barium Titanate Powders. *Journal of the European Ceramic Society* **1999**, *19*, 973–977. https://doi.org/10.1016/S0955-2219(98)00356-2.
43. Moon, J.; Suvaci, E.; Morrone, A.; Costantino, S.A.; Adair, J.H. Formation Mechanisms and Morphological Changes during the Hydrothermal Synthesis of $BaTiO_3$ Particles from a Chemically Modified, Amorphous Titanium (Hydrous) Oxide Precursor. *Journal of the European Ceramic Society* **2003**, *23*, 2153–2161. https://doi.org/10.1016/S0955-2219(03)00016-5.
44. Brown, W.E.; Dollimore, D.; Galwey, A.C. *Reactions in the Solid State*; Comprehensive Chemical Kinetics; Elsevier: Amsterdam, 1980; Vol. 22;.
45. Hancock, J.D.; Sharp, J.H. Method of Comparing Solid-State Kinetic Data and Its Application to the Decomposition of Kaolinite, Brucite, and $BaCO_3$. *Journal of the American Ceramic Society* **1972**, *55*, 74–77. https://doi.org/10.1111/j.1151-2916.1972.tb11213.x.
46. Kingery, W.D.; Bowen, H.K.; Uhlmann, D.R. *Introduction to Ceramics*; 2nd ed.; John Wiley & Sons, Inc.: New York, London, 1976.
47. Kappadan, S.; Gebreab, T.W.; Thomas, S.; Kalarikkal, N. Tetragonal $BaTiO_3$ Nanoparticles: An Efficient Photocatalyst for the Degradation of Organic Pollutants. *Materials Science in Semiconductor Processing* **2016**, *51*, 42–47. https://doi.org/10.1016/j.mssp.2016.04.019.

48. Kristinaitytė, K.; Dagys, L.; Kausteklis, J.; Klimavicius, V.; Doroshenko, I.; Pogorelov, V.; Valevičienė, N.R.; Balevicius, V. NMR and FTIR Studies of Clustering of Water Molecules: From Low-Temperature Matrices to Nano-Structured Materials Used in Innovative Medicine. *Journal of Molecular Liquids* **2017**, *235*, 1–6. https://doi.org/10.1016/j.molliq.2016.11.076.
49. Chizallet, C.; Costentin, G.; Che, M.; Delbecq, F.; Sautet, P. Infrared Characterization of Hydroxyl Groups on MgO: A Periodic and Cluster Density Functional Theory Study. *J. Am. Chem. Soc.* **2007**, *129*, 6442–6452. https://doi.org/10.1021/ja068720e.
50. Fang, C.; Zhou, D.; Gong, S. Core-Shell Structure and Size Effect in Barium Titanate Nanoparticle. *Physica B: Condensed Matter* **2011**, *406*, 1317–1322. https://doi.org/10.1016/j.physb.2011.01.024.
51. Fang, C.; Zhou, D.; Gong, S.; Luo, W. Multishell Structure and Size Effect of Barium Titanate Nanoceramics Induced by Grain Surface Effects: Multishell Structure and Size Effect of Barium Titanate Nanoceramics. *phys. stat. sol. (b)* **2010**, *247*, 219–224. https://doi.org/10.1002/pssb.200945421.
52. Hoshina, T. Size Effect of Barium Titanate: Fine Particles and Ceramics. *J. Ceram. Soc. Japan* **2013**, *121*, 156–161. https://doi.org/10.2109/jcersj2.121.156.
53. Bäurer, M.; Shih, S.-J.; Bishop, C.; Harmer, M.P.; Cockayne, D.; Hoffmann, M.J. Abnormal Grain Growth in Undoped Strontium and Barium Titanate. *Acta Materialia* **2010**, *58*, 290–300. https://doi.org/10.1016/j.actamat.2009.09.007.
54. Li, X.; Yao, Z.; Xie, J.; Li, Z.; Hao, H.; Cao, M.; Ullah, A.; Ullah, A.; Manan, A.; Liu, H. Grain Boundary Effects on Piezoelectric Properties of the Core–Shell-Structured $BaTiO_3$@TiO_2 Ceramics. *J. Adv. Dielect.* **2018**, *08*, 1850044. https://doi.org/10.1142/S2010135X18500443.
55. Curecheriu, L.; Balmus, S.; Buscaglia, M.T.; Buscaglia, V.; Ianculescu, A.; Mitoseriu, L. Grain Size-Dependent Properties of Dense Nanocrystalline Barium Titanate Ceramics. *J. Am. Ceram. Soc.* **2012**, *95*, 3912–3921. https://doi.org/10.1111/j.1551-2916.2012.05409.x.
56. Liu, X.; Li, Z.; Wang, J.; Zhang, R.; Ali, W.; Wang, S.; Lu, X.; Li, C. Phase Equilibria and Thermodynamic Evaluation of BaO-TiO_2-$YO_{1.5}$ System. *Journal of the European Ceramic Society* **2018**, *38*, 5430–5441. https://doi.org/10.1016/j.jeurceramsoc.2018.08.028.
57. Lee, S.; Randall, C.A.; Liu, Z. Modified Phase Diagram for the Barium Oxide–Titanium Dioxide System for the Ferroelectric Barium Titanate. *Journal of the American Ceramic Society* **2007**, *90*, 2589–2594. https://doi.org/10.1111/j.1551-2916.2007.01794.x.
58. Mudiyanselage, K.; Yi, C.-W.; Szanyi, J. Reactivity of a Thick BaO Film Supported on Pt(111): Adsorption and Reaction of NO_2 , H_2O, and CO_2. *Langmuir* **2009**, *25*, 10820–10828. https://doi.org/10.1021/la901371g.
59. Kwon, Soonchul; Lee, Wang-Ro; Lee, Han-Na; Lee, Hanlim Competitive Adsorption of CO_2 and H_2O Molecules on the BaO (100) Surface: A First-Principle Study. *Bulletin of the Korean Chemical Society* **2011**, *32*, 988–992. https://doi.org/10.5012/BKCS.2011.32.3.988.
60. Yi, C.-W.; Szanyi, J. Interaction of D_2O with a Thick BaO Film: Formation of and Phase Transitions in Barium Hydroxides. *J. Phys. Chem. C* **2009**, *113*, 15692–15697. https://doi.org/10.1021/jp903798z.
61. Vittadini, A.; Casarin, M.; Selloni, A. Hydroxylation of TiO_2-B: Insights from Density Functional Calculations. *J. Mater. Chem.* **2010**, *20*, 5871. https://doi.org/10.1039/c0jm00422g.
62. Boldyrev, V.V. Topochemistry and Topochemical Reactions. *Reactivity of Solids* **1990**, *8*, 231–246. https://doi.org/10.1016/0168-7336(90)80023-D.
63. Hertl, W. Kinetics of Barium Titanate Synthesis. *Journal of the American Ceramic Society* **1988**, *71*, 879–883. https://doi.org/10.1111/j.1151-2916.1988.tb07540.x.
64. Kozawa, T.; Onda, A.; Yanagisawa, K. Accelerated Formation of Barium Titanate by Solid-State Reaction in Water Vapour Atmosphere. *Journal of the European Ceramic Society* **2009**, *29*, 3259–3264. https://doi.org/10.1016/j.jeurceramsoc.2009.05.031.
65. Lu, W.; Quilitz, M.; Schmidt, H. Nanoscaled $BaTiO_3$ Powders with a Large Surface Area Synthesized by Precipitation from Aqueous Solutions: Preparation, Characterization and Sintering. *Journal of the European Ceramic Society* **2007**, *27*, 3149–3159. https://doi.org/10.1016/j.jeurceramsoc.2007.01.002.
66. Huan, Y.; Wang, X.; Fang, J.; Li, L. Grain Size Effect on Piezoelectric and Ferroelectric Properties of $BaTiO_3$ Ceramics. *Journal of the European Ceramic Society* **2014**, *34*, 1445–1448. https://doi.org/10.1016/j.jeurceramsoc.2013.11.030.
67. Polotai, A.; Breece, K.; Dickey, E.; Randall, C.; Ragulya, A. A Novel Approach to Sintering Nanocrystalline Barium Titanate Ceramics. *Journal of the American Ceramic Society* **2005**, *88*, 3008–3012. https://doi.org/10.1111/j.1551-2916.2005.00552.x.

68. Kim, H.T.; Han, Y.H. Sintering of Nanocrystalline $BaTiO_3$. *Ceramics International* **2004**, *30*, 1719–1723. https://doi.org/10.1016/j.ceramint.2003.12.141.
69. Radhakrishnan, J.; Subramani, S.; Ocaña, J.L. Cold Sintering Behaviors of Barium Titanates: Recent Progress and Impact on Microstructure, Densification and Dielectric-Ferroelectric Response. *Coordination Chemistry Reviews* **2024**, *502*, 215621. https://doi.org/10.1016/j.ccr.2023.215621.
70. Smirnov, A.V.; Ivakin, Yu.D.; Kornyushin, M.V.; Stolyarov, V.V. The Cold Sintering Process of ZnO and $BaTiO_3$ Ceramics under the Electric Current Influence. *J. Phys.: Conf. Ser.* **2021**, *1967*, 012020. https://doi.org/10.1088/1742-6596/1967/1/012020.
71. Kang, S.; Guo, H.; Wang, J.; Zhong, X.; Li, B. Influence of Surface Coating on the Microstructures and Dielectric Properties of $BaTiO_3$ Ceramic *via* a Cold Sintering Process. *RSC Adv.* **2020**, *10*, 30870–30879. https://doi.org/10.1039/D0RA03849K.
72. Siddiqui, M.; Valášek, D.; Bai, Y.; Salamon, D. Phase Transformation of Cold-Sintered Doped Barium Titanate Ceramics during the Post-Annealing Process. *Open Ceramics* **2023**, *15*, 100401. https://doi.org/10.1016/j.oceram.2023.100401.
73. George, C.N.; Thomas, J.K.; Kumar, H.P.; Suresh, M.K.; Kumar, V.R.; Wariar, P.R.S.; Jose, R.; Koshy, J. Characterization, Sintering and Dielectric Properties of Nanocrystalline Barium Titanate Synthesized through a Modified Combustion Process. *Materials Characterization* **2009**, *60*, 322–326. https://doi.org/10.1016/j.matchar.2008.09.012.
74. Wu, L.; Chure, M.-C.; Wu, K.-K.; Chang, W.-C.; Yang, M.-J.; Liu, W.-K.; Wu, M.-J. Dielectric Properties of Barium Titanate Ceramics with Different Materials Powder Size. *Ceramics International* **2009**, *35*, 957–960. https://doi.org/10.1016/j.ceramint.2008.04.030.
75. Simon-Seveyrat, L.; Hajjaji, A.; Emziane, Y.; Guiffard, B.; Guyomar, D. Re-Investigation of Synthesis of $BaTiO_3$ by Conventional Solid-State Reaction and Oxalate Coprecipitation Route for Piezoelectric Applications. *Ceramics International* **2007**, *33*, 35–40. https://doi.org/10.1016/j.ceramint.2005.07.019.
76. Vinothini, V.; Singh, P.; Balasubramanian, M. Synthesis of Barium Titanate Nanopowder Using Polymeric Precursor Method. *Ceramics International* **2006**, *32*, 99–103. https://doi.org/10.1016/j.ceramint.2004.12.012.
77. Ying, K.-L.; Hsieh, T.-E. Sintering Behaviors and Dielectric Properties of Nanocrystalline Barium Titanate. *Materials Science and Engineering: B* **2007**, *138*, 241–245. https://doi.org/10.1016/j.mseb.2007.01.002.
78. Ismail, F.A.; Maulat Osman, R.A.; Idris, M.S.; Taking, S.; Zahid Jamal, Z.A. Dielectric and Microstructural Properties of $BaTiO_3$ and $Ba_{0.9925}Er_{0.0075}TiO_3$ Ceramics. *EPJ Web Conf.* **2017**, *162*, 01051. https://doi.org/10.1051/epjconf/201716201051.
79. Hu, S.; Luo, C.; Li, P.; Hu, J.; Li, G.; Jiang, H.; Zhang, W. Effect of Sintered Temperature on Structural and Piezoelectric Properties of Barium Titanate Ceramic Prepared by Nano-Scale Precursors. *J Mater Sci: Mater Electron* **2017**, *28*, 9322–9327. https://doi.org/10.1007/s10854-017-6670-7.
80. Kholodkova, A.A.; Danchevskaya, M.N.; Ivakin, Yu.D.; Muravieva, G.P.; Smirnov, A.D.; Tarasovskii, V.P.; Ponomarev, S.G.; Fionov, A.S.; Kolesov, V.V. Properties of Barium Titanate Ceramics Based on Powder Synthesized in Supercritical Water. *Ceramics International* **2018**, *44*, 13129–13138. https://doi.org/10.1016/j.ceramint.2018.04.135.
81. Gates-Rector, S.; Blanton, T. The Powder Diffraction File: A Quality Materials Characterization Database. *Powder Diffr.* **2019**, *34*, 352–360. https://doi.org/10.1017/S0885715619000812.
82. Toby, B.H. *EXPGUI* , a Graphical User Interface for *GSAS*. *J Appl Crystallogr* **2001**, *34*, 210–213. https://doi.org/10.1107/S0021889801002242.
83. Rodríguez-Carvajal, J. Recent Advances in Magnetic Structure Determination by Neutron Powder Diffraction. *Physica B: Condensed Matter* **1993**, *192*, 55–69. https://doi.org/10.1016/0921-4526(93)90108-I.
84. Vaitkus, A.; Merkys, A.; Sander, T.; Quirós, M.; Thiessen, P.A.; Bolton, E.E.; Gražulis, S. A Workflow for Deriving Chemical Entities from Crystallographic Data and Its Application to the Crystallography Open Database. *J Cheminform* **2023**, *15*, 123. https://doi.org/10.1186/s13321-023-00780-2.
85. Rietveld, H.M. A Profile Refinement Method for Nuclear and Magnetic Structures. *J Appl Crystallogr* **1969**, *2*, 65–71. https://doi.org/10.1107/S0021889869006558.